在 CEPC/SppC 上搜寻暗物质

余钊焕

September 10, 2014

1 CEPC

在 CEPC 上, 可以通过 monophoton 信号寻找暗物质粒子 (χ) 产生过程 $e^+e^- \to \chi\bar{\chi}\gamma$. 主要标准模型背景为 $e^+e^- \to \nu\bar{\nu}\gamma$. 下面假设暗物质粒子为 Dirac 费米子, 通过如下 dim-6 算符与电子发生相互作用:

$$\mathcal{O}_e = \frac{1}{\Lambda^2}\bar{\chi}\Gamma_\chi\chi\bar{e}\Gamma_e e, \tag{1}$$

其中 $\Gamma_\chi, \Gamma_e \in \{1, \gamma_5, \gamma^\mu, \gamma^\mu\gamma_5, \sigma^{\mu\nu}\}$.

在 $\sqrt{s} = 250$ GeV 的正负电子对撞机上, 事例筛选条件如下.

- A monophoton with $E_\gamma > 10$ GeV and $15° < \theta_\gamma < 165°$.
- No any other particle.
- $m_{\text{rec}} \geq 120$ GeV, where the recoil mass is defined as $m_{\text{rec}} \equiv \sqrt{(p_{e^-} + p_{e^+} - p_\gamma)^2}$ with p_{e^-} (p_{e^-}) denoting the 4-momentum of the beam e^- (e^+).

经过事例筛选后, 背景 $e^+e^- \to \nu\bar{\nu}\gamma$ 的截面为 1250 fb. 对暗物质信号的探测能力如 Fig. 1 所示.

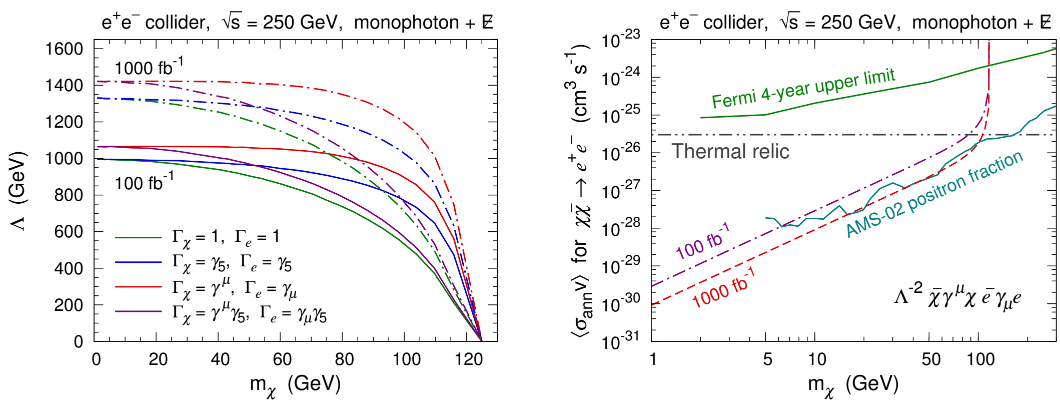

(a) m_χ-Λ plane.

(b) m_χ-$\langle\sigma_{\text{ann}}v\rangle$ plane.

Figure 1: 在 CEPC 上探测暗物质粒子的 3σ 灵敏度曲线. 图中还标出 Fermi-LAT 对矮星系的 γ 射线观测给出的 95% 置信度上限 [1]. 以及由 AMS-02 的正电子比例能谱给出的 95% 置信度上限 [2].

2 SppC

2.1 有效算符

在 SppC 上, 可以通过 monojet 信号寻找暗物质粒子 (χ) 产生过程 $pp \to \chi\bar{\chi} + \text{jets}$. 在 33 TeV 和 100 TeV 对撞机上的相关 snowmass 研究参见 [3]. $pp \to Z(\to \nu\bar{\nu}) + \text{jets}$ 是不可约背景. $pp \to W(\to \ell\nu) + \text{jets}$ 也是一种背景, 因为末态中的轻子可能被合并到 jet 之中. 下面假设暗物质粒子为 Dirac 费米子, 与六种夸克发生矢量流相互作用

$$\mathcal{O}_{\mathrm{V}} = \frac{1}{\Lambda^2} \sum_q \bar{\chi}\gamma^\mu\chi\bar{q}\gamma_\mu q, \tag{2}$$

或轴矢量流相互作用

$$\mathcal{O}_{\mathrm{A}} = \frac{1}{\Lambda^2} \sum_q \bar{\chi}\gamma^\mu\gamma_5\chi\bar{q}\gamma_\mu\gamma_5 q. \tag{3}$$

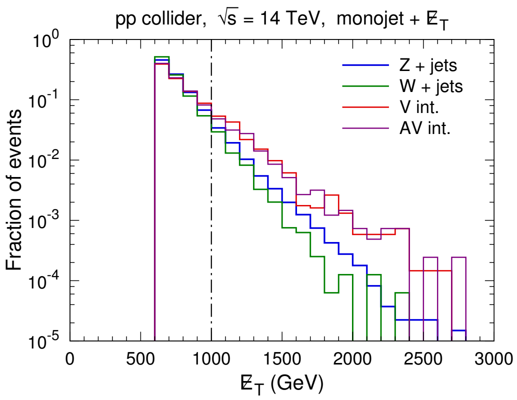

(a) LHC, 14 TeV.

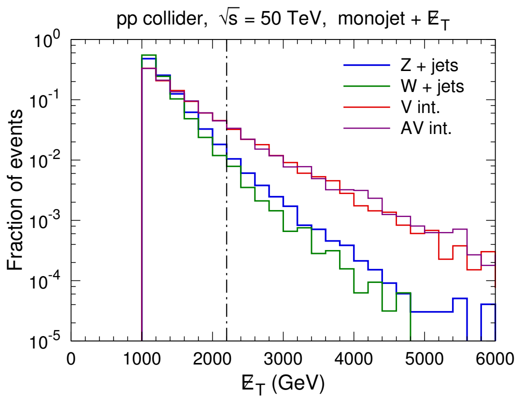

(b) SppC, 50 TeV.

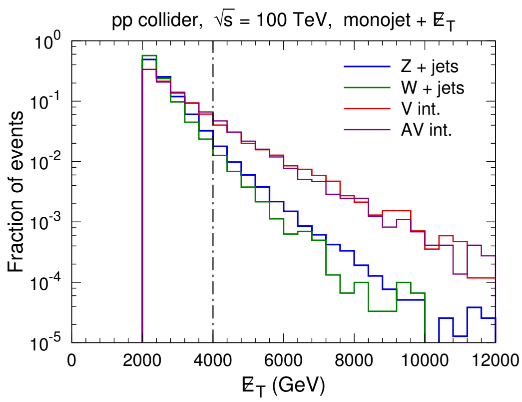

(c) SppC, 100 TeV.

Figure 2: 强子对撞机 monojet 搜寻道信号和背景的归一化 $\not{E}_{\mathrm{T}}$ 分布. 点划线表示筛选条件阈值. 对于矢量流和轴矢量流相互作用, 这里分别假设 $m_\chi = 500$ GeV 和 100 GeV.

我们用 `MadGraph 5`, `PYTHIA 6` 和 `Delphes 3` 进行模拟计算, 用 ATLAS 探测器的参数进行探测器模拟. 对 $\sqrt{s} = 14/50/100$ TeV 的 LHC 或 SppC, 取如下事例筛选条件.

- No more than 2 jets with $p_{\mathrm{T}} > 50/100/200$ GeV and $|\eta| < 4$.

- No any isolated e, μ, τ, and γ with $p_{\mathrm{T}} > 20$ GeV and $|\eta| < 2.5$.
- $\not{E}_{\mathrm{T}} > 1000/2200/4000$ GeV.
- The leading jet satisfies $p_{\mathrm{T}}(j_1) > 1000/2200/4000$ GeV and $|\eta| < 2.4$.
- $\Delta\phi(j_1, j_2) < 2.5$.

最后一条用于压低 QCD multi-jet 背景. 经过事例筛选后, 背景 $Z(\to \nu\bar{\nu})$+jets 的截面为 5.10/5.08/2.13 fb, $W(\to \ell\nu)$ + jets 的截面为 1.53/1.10/0.39 fb. 信号和背景的归一化 $\not{E}_{\mathrm{T}}$ 分布如 Fig. 2 所示. 可以看出, 信号倾向于更大的 $\not{E}_{\mathrm{T}}$. 强子对撞机 monojet 搜寻道 90% 置信度的排除能力如 Figs. 3, 4 和 5 所示.

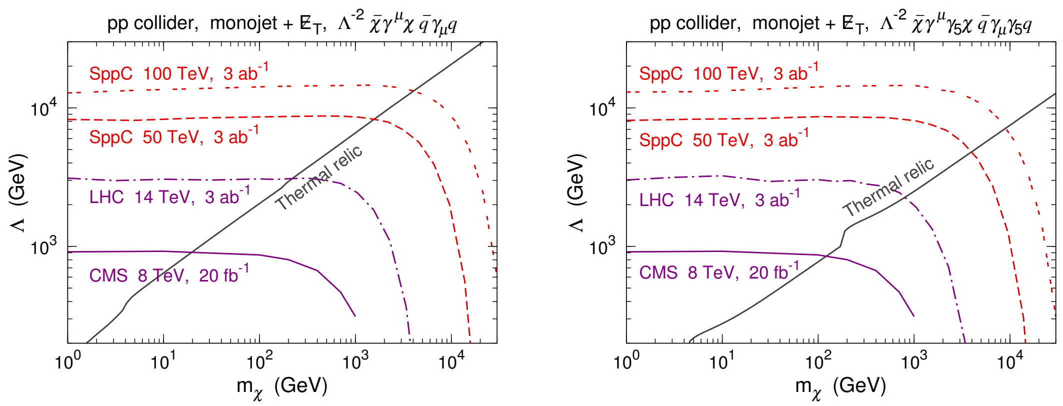

(a) Vector operator.

(b) Axial vector operator.

Figure 3: 在 m_χ-Λ 平面上, 强子对撞机 monojet 搜寻道 90% 置信度的排除能力. 紫色实线表示 CMS 实验组分析的 8 TeV LHC 排除限 [4]. 灰色实线表示可以得出正确 relic density 的参数值 [5].

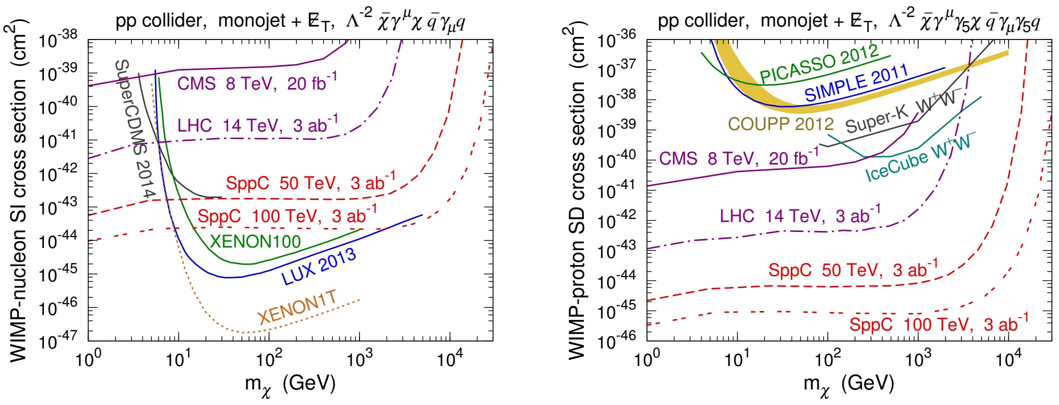

(a) Vector operator, spin-independent.

(b) Axial vector operator, spin-dependent.

Figure 4: 转换到暗物质粒子与核子散射截面上, 强子对撞机 monojet 搜寻道 90% 置信度的排除能力. 紫色实线表示 CMS 实验组分析的 8 TeV LHC 排除限 [4]. 对于自旋无关散射, 图中标示了直接探测实验 XENON100 [6], LUX [7] 和 SuperCDMS [8] 的排除限, 以及 XENON1T [9] 的预期探测能力. 对于自旋相关散射, 图中标示了直接探测实验 SIMPLE [10], PICASSO [11] 和 COUPP [12] 的排除限, 以及中微子探测实验 Super-K [13] 和 IceCube [14] 的排除限.

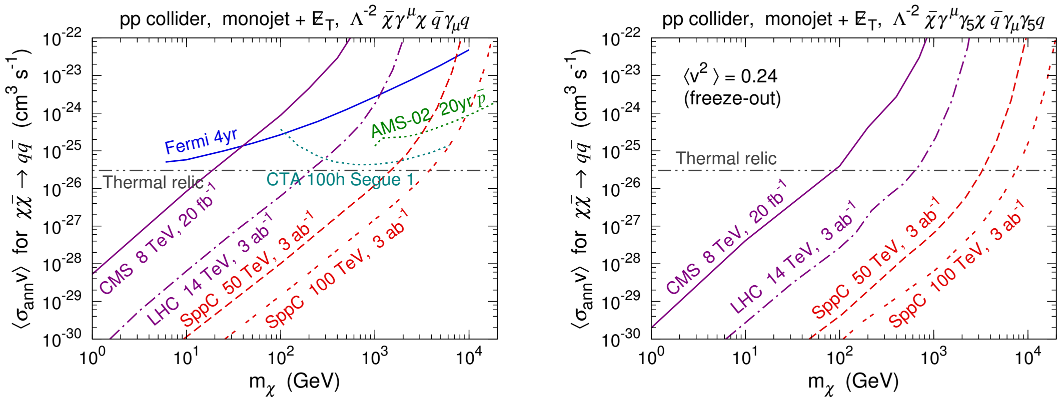

(a) Vector operator. (b) Axial vector operator.

Figure 5: 转换到暗物质粒子湮灭到 6 种夸克的截面上, 强子对撞机 monojet 搜寻道 90% 置信度的排除能力. 对于 s 波湮灭受到螺旋度压低的轴矢量流相互作用, 为与 thermal relic 标准湮灭截面值比较, 取暗物质 freeze-out 时期的速度弥散值 $\langle v^2\rangle = 0.24$ 进行计算 (参考 [15]). 紫色实线表示 CMS 实验组分析的 8 TeV LHC 排除限 [4]. 图中还标示了 Fermi-LAT 对矮星系的 γ 射线观测给出的 95% 置信度上限 [1], 以及 CTA [16] 对矮星系 Segue 1 γ 射线观测和 AMS02 反质子能谱观测的预期探测能力.

2.2 Z' 模型

下面讨论暗物质与夸克的相互作用通过一个 Z' 粒子传递的情况, 相关研究可以参考文献 [3, 17]. 分别假设 Z' 粒子为矢量粒子和轴矢量粒子, 与 Dirac 暗物质粒子和夸克有如下耦合:

$$\mathcal{L}_{\rm V} = \left(\sum_q g_q\bar{q}\gamma_\mu q + g_\chi\bar{\chi}\gamma_\mu\chi\right) Z'^\mu, \tag{4}$$

$$\mathcal{L}_{\rm A} = \left(\sum_q g_q\bar{q}\gamma_\mu\gamma_5 q + g_\chi\bar{\chi}\gamma_\mu\gamma_5\chi\right) Z'^\mu. \tag{5}$$

在计算中, 还假设 Z' 与各种夸克的耦合 g_q 是相同的.

对 $\sqrt{s} = 14/50$ TeV 的 LHC 或 SppC, 取如下事例筛选条件.

- No more than 2 jets with $p_{\rm T} > 50/100$ GeV and $|\eta| < 4$.
- No any isolated e, μ, τ, and γ with $p_{\rm T} > 20$ GeV and $|\eta| < 2.5$.
- $\not{E}_{\rm T} > 900/1800$ GeV.
- The leading jet satisfies $p_{\rm T}(j_1) > 900/1800$ GeV and $|\eta| < 2.4$.
- $\Delta\phi(j_1, j_2) < 2.5$.

经过事例筛选后, 背景 $Z(\to \nu\bar{\nu}) + \text{jets}$ 的截面为 9.47/14.3 fb, $W(\to \ell\nu) + \text{jets}$ 的截面为 3.02/3.38 fb. 信号和背景的归一化 $\not{E}_{\rm T}$ 分布如 Fig. 6 所示. 强子对撞机 monojet 搜寻道 90% 置信度的排除能力如 Figs. 7, 8 和 9 所示.

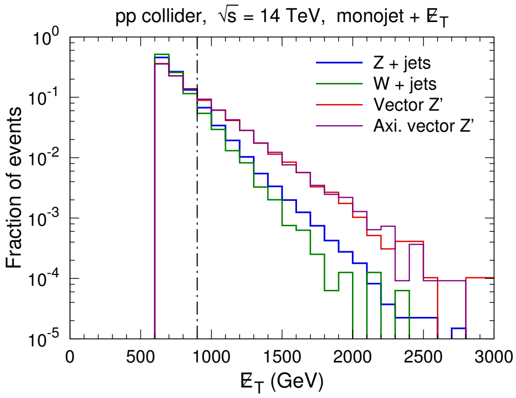

(a) LHC, 14 TeV.

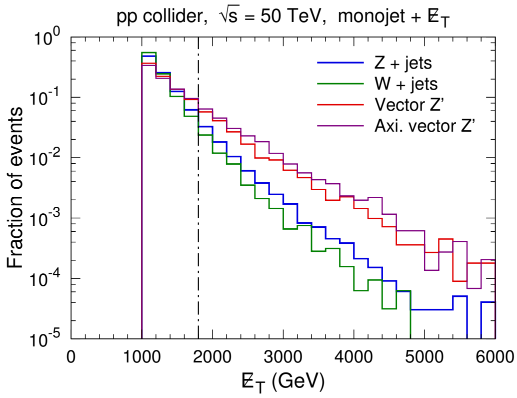

(b) SppC, 50 TeV.

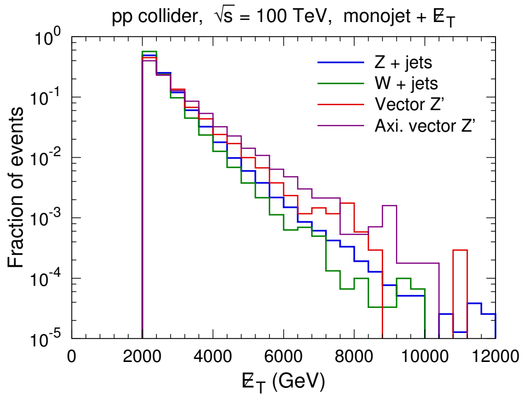

(c) SppC, 100 TeV.

Figure 6: 对于 Z' 模型, 强子对撞机 monojet 搜寻道信号和背景的归一化 $\not{E}_T$ 分布. 点划线表示筛选条件阈值. 对于矢量 (轴矢量) Z' 粒子, 这里假设 $m_{Z'} = 3$ TeV 和 $m_\chi = 300$ (1600) GeV.

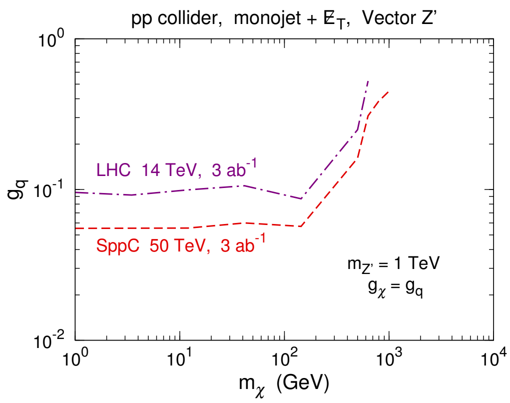

(a) Vector Z'.

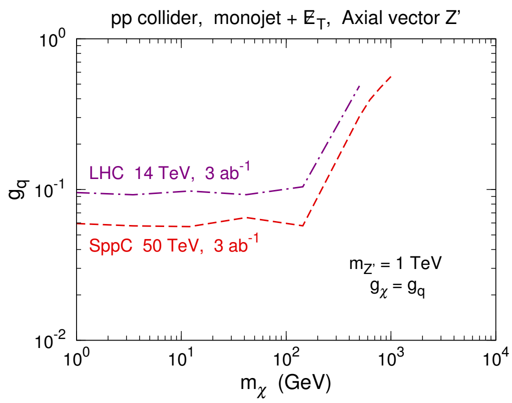

(b) Axial vector Z'.

Figure 7: 对于 Z' 模型, 在 m_χ-g_q 平面上, 强子对撞机 monojet 搜寻道 90% 置信度的排除能力. 这里假设 $m_{Z'} = 1$ TeV 且 $g_\chi = g_q$.

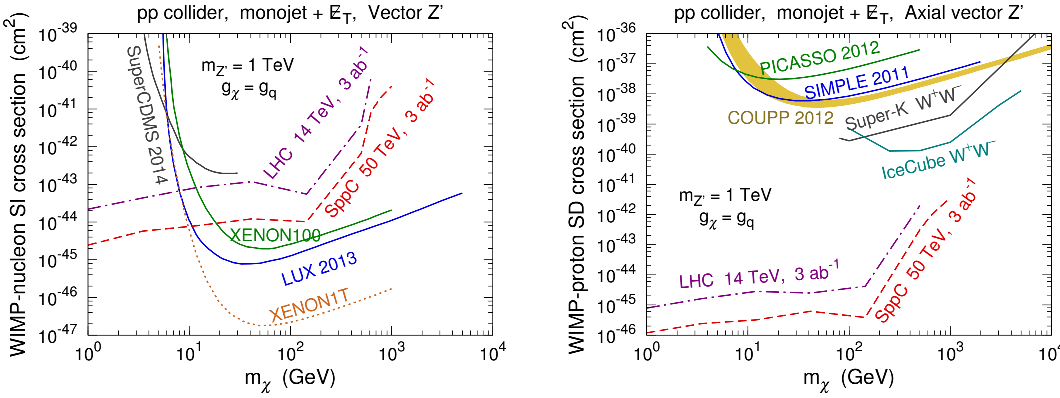

(a) Vector Z', spin-independent.

(b) Axial vector Z', spin-dependent.

Figure 8: 对于 Z' 模型, 转换到暗物质粒子与核子散射截面上, 强子对撞机 monojet 搜寻道 90% 置信度的排除能力. 这里假设 $m_{Z'} = 1$ TeV 且 $g_\chi = g_q$.

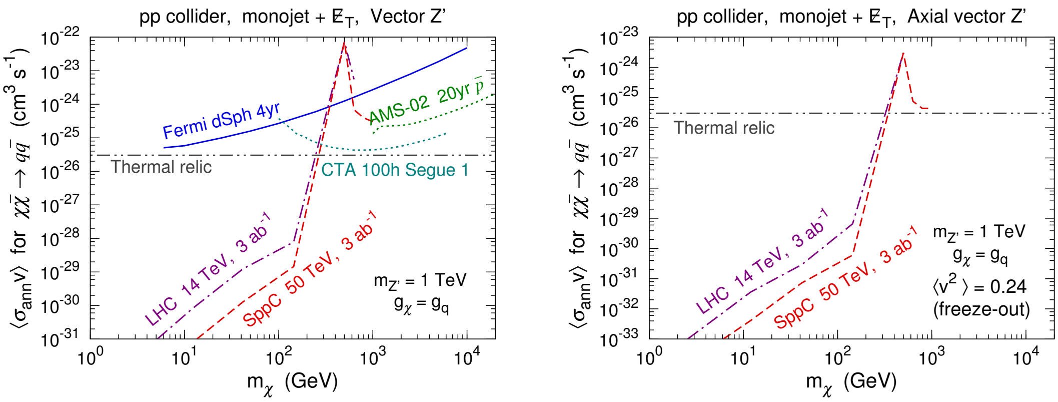

(a) Vector Z'.

(b) Axial vector Z'.

Figure 9: 对于 Z' 模型, 转换到暗物质粒子湮灭到 6 种夸克的截面上, 强子对撞机 monojet 搜寻道 90% 置信度的排除能力. 对于 s 波湮灭受到螺旋度压低的轴矢量流相互作用, 为与 thermal relic 标准湮灭截面值比较, 取暗物质 freeze-out 时期的速度弥散值 $\langle v^2 \rangle = 0.24$ 进行计算 (参考 [15]). 这里假设 $m_{Z'} = 1$ TeV 且 $g_\chi = g_q$.

A Z' 模型截面计算

对于这里考虑的两种 Z' 模型, 暗物质与原子核的散射截面可以参考文献 [17].

由于暗物质湮灭截面的计算依赖于 Z' 的宽度, 这里先计算宽度. 对于衰变过程 $Z'(p) \to q(k_1) + \bar{q}(k_2)$, 有如下运动学关系.

$$\begin{aligned} k_1^0 &= k_2^0 = \frac{m_{Z'}}{2}, \quad |\mathbf{k}_1| = |\mathbf{k}_2| = \frac{m_{Z'}}{2}\sqrt{1 - 4m_q^2/m_{Z'}^2} = \frac{m_{Z'}}{2}\xi_q, \quad \xi_q \equiv \sqrt{1 - 4m_q^2/m_{Z'}^2}, & (6) \\ m_{Z'}^2 &= p^2 = (k_1 + k_2)^2 = 2m_q^2 + 2k_1 \cdot k_2, \quad m_q^2 = k_1^2 = (p - k_2)^2 = m_{Z'}^2 + m_q^2 - 2p \cdot k_2, & (7) \\ k_1 \cdot k_2 &= \frac{m_{Z'}^2}{2}(1 - 2m_q^2/m_{Z'}^2), \quad p \cdot k_1 = p \cdot k_2 = \frac{m_{Z'}^2}{2}. & (8) \end{aligned}$$

对于矢量 Z' 粒子, 不变振幅为

$$i\mathcal{M} = ig_q \bar{u}(k_1)\gamma_\mu v(k_2)\varepsilon^\mu(p), \quad (i\mathcal{M})^* = -ig_q \bar{v}(k_2)\gamma_\nu u(k_1)\varepsilon^{\nu*}(p). \tag{9}$$

则

$$\begin{aligned} \frac{1}{3}\sum_{\text{spins}} |\mathcal{M}|^2 &= \sum_{\text{spins}} \frac{g_q^2}{3}\bar{u}(k_1)\gamma_\mu v(k_2)\bar{v}(k_2)\gamma_\nu u(k_1)\varepsilon^\mu(p)\varepsilon^{\nu*}(p) \\ &= \frac{g_q^2}{3}\mathrm{Tr}[(\not{k}_1 + m_q)\gamma_\mu(\not{k}_2 - m_q)\gamma_\nu]\left(-g^{\mu\nu} + \frac{p^\mu p^\nu}{m_{Z'}^2}\right) \\ &= \frac{4}{3}g_q^2 m_{Z'}^2(1 + 2m_q^2/m_{Z'}^2). \end{aligned} \tag{10}$$

于是, Z' 衰变到一对夸克的宽度为

$$\Gamma_{Z' \to q\bar{q}} = \frac{1}{8\pi}\frac{|\mathbf{k}_1|}{m_{Z'}^2} c_q \frac{1}{3}\sum_{\text{spins}} |\mathcal{M}|^2 = \frac{\xi_q}{16\pi m_{Z'}} c_q \frac{1}{3}\sum_{\text{spins}} |\mathcal{M}|^2 = \frac{c_q g_q^2}{12\pi} m_{Z'}\xi_q(1 + 2m_q^2/m_{Z'}^2), \tag{11}$$

其中 $c_q = 3$, 是夸克的颜色因子. 同理, Z' 衰变到一对暗物理粒子的宽度为

$$\Gamma_{Z' \to \chi\bar{\chi}} = \frac{g_\chi^2}{12\pi} m_{Z'}\xi_\chi(1 + 2m_\chi^2/m_{Z'}^2). \tag{12}$$

其中 $\xi_\chi \equiv \sqrt{1 - 4m_\chi^2/m_{Z'}^2}$.

对于轴矢量 Z' 粒子, 不变振幅为

$$i\mathcal{M} = ig_q \bar{u}(k_1)\gamma_\mu\gamma_5 v(k_2)\varepsilon^\mu(p), \quad (i\mathcal{M})^* = -ig_q \bar{v}(k_2)\gamma_\nu\gamma_5 u(k_1)\varepsilon^{\nu*}(p). \tag{13}$$

则

$$\begin{aligned} \frac{1}{3}\sum_{\text{spins}} |\mathcal{M}|^2 &= \sum_{\text{spins}} \frac{g_q^2}{3}\bar{u}(k_1)\gamma_\mu\gamma_5 v(k_2)\bar{v}(k_2)\gamma_\nu\gamma_5 u(k_1)\varepsilon^\mu(p)\varepsilon^{\nu*}(p) \\ &= \frac{g_q^2}{3}\mathrm{Tr}[(\not{k}_1 + m_q)\gamma_\mu\gamma_5(\not{k}_2 - m_q)\gamma_\nu\gamma_5]\left(-g^{\mu\nu} + \frac{p^\mu p^\nu}{m_{Z'}^2}\right) \\ &= \frac{4}{3}g_q^2(m_{Z'}^2 - 4m_q^2) = \frac{4}{3}g_q^2 m_{Z'}^2\xi_q^2. \end{aligned} \tag{14}$$

于是, Z' 衰变到一对夸克的宽度为

$$\Gamma_{Z'\to q\bar{q}} = \frac{1}{8\pi}\frac{|\mathbf{k}_1|}{m_{Z'}^2}c_q\frac{1}{3}\sum_{\text{spins}}|\mathcal{M}|^2 = \frac{\xi_q}{16\pi m_{Z'}}c_q\frac{1}{3}\sum_{\text{spins}}|\mathcal{M}|^2 = \frac{c_q g_q^2}{12\pi}m_{Z'}\xi_q^3. \tag{15}$$

同理, Z' 衰变到一对暗物理粒子的宽度为

$$\Gamma_{Z'\to\chi\bar{\chi}} = \frac{g_\chi^2}{12\pi}m_{Z'}\xi_\chi^3. \tag{16}$$

Z' 粒子的总宽度可表达为

$$\Gamma_{Z'} = \sum_q \Gamma_{Z'\to q\bar{q}} + \Gamma_{Z'\to\chi\bar{\chi}}. \tag{17}$$

Z' 粒子的宽度随耦合系数 g_q 和质量 $m_{Z'}$ 的变化关系如 Fig. 10 如示.

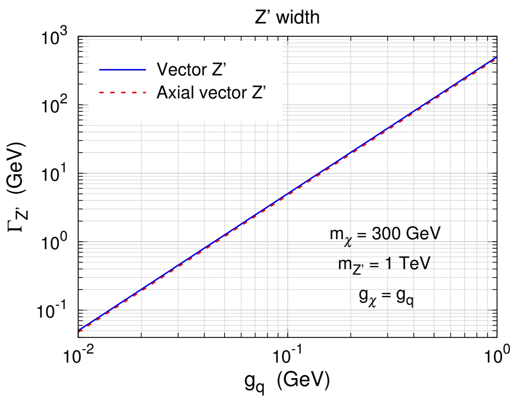

(a) Z' 粒子的宽度与耦合系数 g_q 的关系.

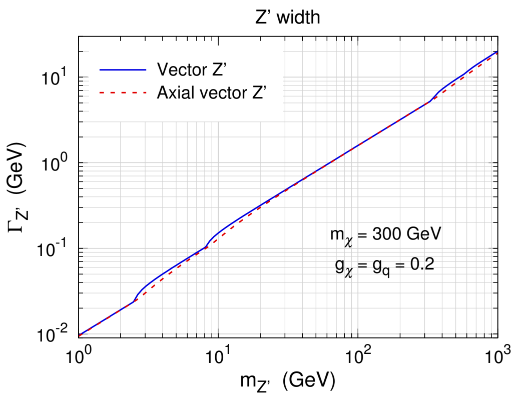

(b) Z' 粒子的宽度与质量 $m_{Z'}$ 的关系.

Figure 10: Z' 粒子的宽度随耦合系数 g_q 和质量 $m_{Z'}$ 的变化关系. 这里假设 $g_\chi = g_q$.

下面计算暗物质湮灭截面. 对于湮灭过程 $\chi(p_1)+\bar{\chi}(p_2)\to q(k_1)+\bar{q}(k_2)$, 质心系中的运动学关系如下.

$$\begin{aligned}
p_1^0 &= p_2^0 = k_1^0 = k_2^0 = \frac{\sqrt{s}}{2}, \\
p_2\cdot k_1 &= p_1\cdot k_2 = p_1^0 k_1^0 + |\mathbf{p}_1||\mathbf{k}_1|\cos\theta = \frac{s}{4}(1+\beta_\chi\beta_q\cos\theta), \\
\beta_\chi &\equiv \sqrt{1-4m_\chi^2/s}, \quad \beta_\tau \equiv \sqrt{1-4m_\tau^2/s}, \\
p_1\cdot p_2 &= \frac{s}{2}-m_\chi^2, \quad k_1\cdot k_2 = \frac{s}{2}-m_q^2, \\
q = p_1+p_2 &= k_1+k_2, \quad q\cdot p_1 = q\cdot p_2 = q\cdot k_1 = q\cdot k_2 = \frac{s}{2}.
\end{aligned} \tag{18}$$

对于矢量 Z' 粒子, 不变振幅为

$$\begin{aligned}
i\mathcal{M} &= ig_\chi\bar{v}(p_2)\gamma_\mu u(p_1)\frac{-i(g^{\mu\nu}-q^\mu q^\nu/m_{Z'}^2)}{q^2-m_{Z'}^2+im_{Z'}\Gamma_{Z'}}ig_q\bar{u}(k_1)\gamma_\nu v(k_2) \\
&= ig_\chi g_q\frac{g^{\mu\nu}-q^\mu q^\nu/m_{Z'}^2}{s-m_{Z'}^2+im_{Z'}\Gamma_{Z'}}\bar{v}(p_2)\gamma_\mu u(p_1)\bar{u}(k_1)\gamma_\nu v(k_2),
\end{aligned} \tag{19}$$

$$(i\mathcal{M})^* = -ig_\chi g_q\frac{g^{\rho\sigma}-q^\rho q^\sigma/m_{Z'}^2}{s-m_{Z'}^2-im_{Z'}\Gamma_{Z'}}\bar{u}(p_1)\gamma_\rho v(p_2)\bar{v}(k_2)\gamma_\sigma u(k_1). \tag{20}$$

则

$$\begin{aligned}
\frac{1}{4}\sum_{\text{spins}}|\mathcal{M}|^2 &= \sum_{\text{spins}}\frac{(g_\chi g_q)^2}{4[(s-m_{Z'}^2)^2+m_{Z'}^2\Gamma_{Z'}^2]}\left(g^{\mu\nu}-\frac{q^\mu q^\nu}{m_{Z'}^2}\right)\left(g^{\rho\sigma}-\frac{q^\rho q^\sigma}{m_{Z'}^2}\right)\\
&\quad\times\bar{v}(p_2)\gamma_\mu u(p_1)\bar{u}(p_1)\gamma_\rho v(p_2)\bar{u}(k_1)\gamma_\nu v(k_2)\bar{v}(k_2)\gamma_\sigma u(k_1)\\
&= \frac{(g_\chi g_q)^2}{4[(s-m_{Z'}^2)^2+m_{Z'}^2\Gamma_{Z'}^2]}\left(g^{\mu\nu}-\frac{q^\mu q^\nu}{m_{Z'}^2}\right)\left(g^{\rho\sigma}-\frac{q^\rho q^\sigma}{m_{Z'}^2}\right)\\
&\quad\times\mathrm{Tr}[(\not{p}_2-m_\chi)\gamma_\mu(\not{p}_1+m_\chi)\gamma_\rho]\mathrm{Tr}[(\not{k}_1+m_q)\gamma_\nu(\not{k}_2-m_q)\gamma_\sigma]\\
&= \frac{(g_\chi g_q)^2}{(s-m_{Z'}^2)^2+m_{Z'}^2\Gamma_{Z'}^2}s[s(1+\beta_\chi^2\beta_q^2\cos^2\theta)+4m_\chi^2+4m_q^2]. \qquad (21)
\end{aligned}$$

由

$$\frac{d\sigma_{\text{ann}}}{d\Omega}=\frac{1}{2p_1^0 2p_2^0|\mathbf{v}_1-\mathbf{v}_2|}\frac{|\mathbf{k}_1|}{(2\pi)^2 4E_{\text{CM}}}c_q\frac{1}{4}\sum_{\text{spins}}|\mathcal{M}|^2=\frac{c_q\beta_q}{64\pi^2 s\beta_\chi}\frac{1}{4}\sum_{\text{spins}}|\mathcal{M}|^2, \qquad (22)$$

可得湮灭截面

$$\begin{aligned}
\sigma_{\text{ann}} &= \frac{c_q\beta_q}{64\pi^2 s\beta_\chi}2\pi\int d\cos\theta\frac{1}{4}\sum_{\text{spins}}|\mathcal{M}|^2=\frac{c_q\beta_q}{32\pi s\beta_\chi}\int d\cos\theta\frac{1}{4}\sum_{\text{spins}}|\mathcal{M}|^2\\
&= \frac{c_q\beta_q}{12\pi\beta_\chi}\frac{(g_\chi g_q)^2 s}{(s-m_{Z'}^2)^2+m_{Z'}^2\Gamma_{Z'}^2}\left(1+2\frac{m_q^2}{s}\right)\left(1+2\frac{m_\chi^2}{s}\right). \qquad (23)
\end{aligned}$$

对 s 作速度展开, $s\simeq 4m_\chi^2+m_\chi^2v^2+\frac{3}{4}m_\chi^2v^4$ [5], 可将 $\sigma_{\text{ann}}v$ 展开为 $\sigma_{\text{ann}}v\simeq a+bv^2$ 的形式. 求得

$$\begin{aligned}
a &= \frac{c_q g_q^2 g_\chi^2\sqrt{1-m_q^2/m_\chi^2}(m_q^2+2m_\chi^2)}{2\pi[(m_{Z'}^2-4m_\chi^2)^2+m_{Z'}^2\Gamma_{Z'}^2]},\\
b &= \frac{c_q g_q^2 g_\chi^2}{48\pi m_\chi^2\sqrt{1-m_q^2/m_\chi^2}[(m_{Z'}^2-4m_\chi^2)^2+m_{Z'}^2\Gamma_{Z'}^2]^2}\{m_{Z'}^2\Gamma_{Z'}^2(2m_q^2m_\chi^2+11m_q^4-4m_\chi^4)\\
&\quad+(m_{Z'}^2-4m_\chi^2)[-4m_\chi^4(14m_q^2+m_{Z'}^2)+2m_q^2m_\chi^2(m_{Z'}^2-46m_q^2)+11m_q^4m_{Z'}^2+112m_\chi^6]\}. \qquad (24)
\end{aligned}$$

对于轴矢量 Z' 粒子, 不变振幅为

$$\begin{aligned}
i\mathcal{M} &= ig_\chi\bar{v}(p_2)\gamma_\mu\gamma_5 u(p_1)\frac{-i(g^{\mu\nu}-q^\mu q^\nu/m_{Z'}^2)}{q^2-m_{Z'}^2+im_{Z'}\Gamma_{Z'}}ig_q\bar{u}(k_1)\gamma_\nu\gamma_5 v(k_2)\\
&= ig_\chi g_q\frac{g^{\mu\nu}-q^\mu q^\nu/m_{Z'}^2}{s-m_{Z'}^2+im_{Z'}\Gamma_{Z'}}\bar{v}(p_2)\gamma_\mu\gamma_5 u(p_1)\bar{u}(k_1)\gamma_\nu\gamma_5 v(k_2),\\
(i\mathcal{M})^* &= -ig_\chi g_q\frac{g^{\rho\sigma}-q^\rho q^\sigma/m_{Z'}^2}{s-m_{Z'}^2-im_{Z'}\Gamma_{Z'}}\bar{u}(p_1)\gamma_\rho\gamma_5 v(p_2)\bar{v}(k_2)\gamma_\sigma\gamma_5 u(k_1). \qquad (25)
\end{aligned}$$

则

$$\begin{aligned}
&\frac{1}{4}\sum_{\text{spins}}|\mathcal{M}|^2\\
&= \sum_{\text{spins}}\frac{(g_\chi g_q)^2}{4[(s-m_{Z'}^2)^2+m_{Z'}^2\Gamma_{Z'}^2]}\left(g^{\mu\nu}-\frac{q^\mu q^\nu}{m_{Z'}^2}\right)\left(g^{\rho\sigma}-\frac{q^\rho q^\sigma}{m_{Z'}^2}\right)
\end{aligned}$$

$$
\begin{aligned}
&\times\bar{v}(p_2)\gamma_\mu\gamma_5 u(p_1)\bar{u}(p_1)\gamma_\rho\gamma_5 v(p_2)\bar{u}(k_1)\gamma_\nu\gamma_5 v(k_2)\bar{v}(k_2)\gamma_\sigma\gamma_5 u(k_1)\\
=\ &\frac{(g_\chi g_q)^2}{4[(s-m_{Z'}^2)^2+m_{Z'}^2\Gamma_{Z'}^2]}\left(g^{\mu\nu}-\frac{q^\mu q^\nu}{m_{Z'}^2}\right)\left(g^{\rho\sigma}-\frac{q^\rho q^\sigma}{m_{Z'}^2}\right)\\
&\times\mathrm{Tr}[(\not{p}_2-m_\chi)\gamma_\mu\gamma_5(\not{p}_1+m_\chi)\gamma_\rho\gamma_5]\mathrm{Tr}[(\not{k}_1+m_q)\gamma_\nu\gamma_5(\not{k}_2-m_q)\gamma_\sigma\gamma_5]\\
=\ &\frac{(g_\chi g_q)^2}{(s-m_{Z'}^2)^2+m_{Z'}^2\Gamma_{Z'}^2}[s^2(1+\beta_\chi^2\beta_q^2\cos^2\theta)-4m_\chi^2 s\\
&\quad -4m_q^2 s+32m_\chi^2 m_q^2-32m_q^2 m_\chi^2 s/m_{Z'}^2+16m_q^2 m_\chi^2 s^2/m_{Z'}^2]\\
=\ &\frac{(g_\chi g_q)^2}{(s-m_{Z'}^2)^2+m_{Z'}^2\Gamma_{Z'}^2}\left[s^2(1+\beta_\chi^2\beta_q^2\cos^2\theta)-4m_\chi^2 s-4m_q^2 s+16m_q^2 m_\chi^2\left(2-2\frac{s}{m_{Z'}^2}+\frac{s^2}{m_{Z'}^4}\right)\right].
\end{aligned}\tag{26}
$$

湮灭截面

$$
\begin{aligned}
\sigma_{\rm ann}\ =\ &\frac{c_q\beta_q}{32\pi s\beta_\chi}\int d\cos\theta\frac{1}{4}\sum_{\rm spins}|\mathcal{M}|^2\\
=\ &\frac{c_q\beta_q}{48\pi\beta_\chi}\frac{(g_\chi g_q)^2 s}{(s-m_{Z'}^2)^2+m_{Z'}^2\Gamma_{Z'}^2}\left(3+\beta_\chi^2\beta_q^2-12\frac{m_\chi^2}{s}-12\frac{m_q^2}{s}+96\frac{m_q^2m_\chi^2}{s^2}-96\frac{m_q^2m_\chi^2}{sm_{Z'}^2}+48\frac{m_q^2m_\chi^2}{m_{Z'}^4}\right).
\end{aligned}\tag{27}
$$

速度展开的系数为

$$
\begin{aligned}
a\ =\ &\frac{c_q g_q^2 g_\chi^2 m_q^2\sqrt{1-m_q^2/m_\chi^2}(1-4m_\chi^2/m_{Z'}^2)^2}{2\pi[(m_{Z'}^2-4m_\chi^2)^2+m_{Z'}^2\Gamma_{Z'}^2]},\\
b\ =\ &\frac{c_q g_q^2 g_\chi^2}{48\pi m_\chi^2 m_{Z'}^4\sqrt{1-m_q^2/m_\chi^2}[(m_{Z'}^2-4m_\chi^2)^2+m_{Z'}^2\Gamma_{Z'}^2]^2}\\
&\times\{m_{Z'}^2\Gamma_{Z'}^2[-4m_q^2m_\chi^2m_{Z'}^2(18m_q^2+7m_{Z'}^2)+8m_\chi^4(6m_q^2m_{Z'}^2+6m_q^4+m_{Z'}^4)+23m_q^4m_{Z'}^4]\\
&\quad+(m_{Z'}^2-4m_\chi^2)^2[m_q^4(240m_\chi^4-120m_\chi^2m_{Z'}^2+23m_{Z'}^4)\\
&\qquad -4m_q^2(48m_\chi^6-24m_\chi^4m_{Z'}^2+7m_\chi^2m_{Z'}^4)+8m_\chi^4m_{Z'}^4]\}.
\end{aligned}\tag{28}
$$

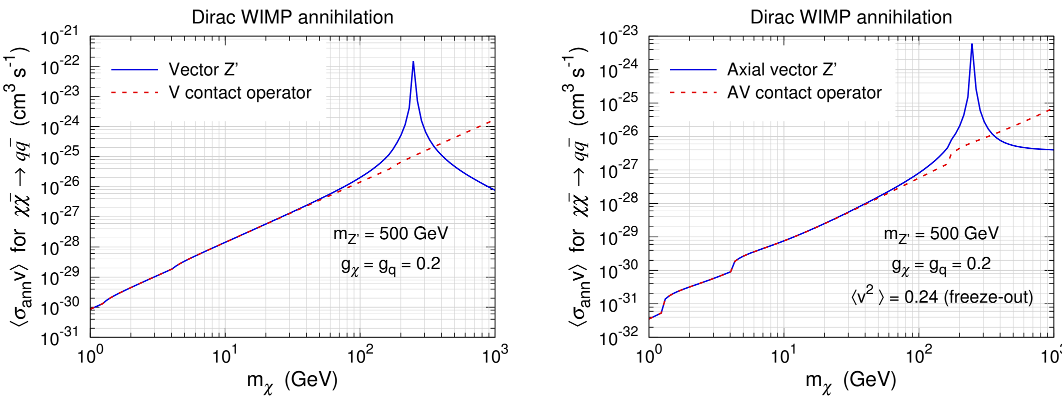

(a) Vector Z'.　　(b) Axial vector Z'.

Figure 11: 在 Z' 模型中, 暗物质湮灭到夸克的截面随质量 m_χ 的变化关系. 这里假设 $m_{Z'}=500$ GeV 且 $g_\chi=g_q$. 图中还画出有效算符的结果加以比较.

参考文献

[1] M. Ackermann *et al.* [Fermi-LAT Collaboration], "Dark Matter Constraints from Observations of 25 Milky Way Satellite Galaxies with the Fermi Large Area Telescope," Phys. Rev. D **89**, 042001 (2014) [arXiv:1310.0828 [astro-ph.HE]].

[2] L. Bergstrom, T. Bringmann, I. Cholis, D. Hooper and C. Weniger, "New limits on dark matter annihilation from AMS cosmic ray positron data," Phys. Rev. Lett. **111**, 171101 (2013) [arXiv:1306.3983 [astro-ph.HE]].

[3] N. Zhou, D. Berge, L. Wang, D. Whiteson and T. Tait, "Sensitivity of future collider facilities to WIMP pair production via effective operators and light mediators," arXiv:1307.5327 [hep-ex].

[4] CMS Collaboration, "Search for new physics in monojet events in pp collisions at sqrt(s)= 8 TeV," CMS-PAS-EXO-12-048.

[5] J. -M. Zheng, Z. -H. Yu, J. -W. Shao, X. -J. Bi, Z. Li and H. -H. Zhang, "Constraining the interaction strength between dark matter and visible matter: I. fermionic dark matter," Nucl. Phys. B **854**, 350 (2012) [arXiv:1012.2022 [hep-ph]].

[6] E. Aprile *et al.* [XENON100 Collaboration], "Dark Matter Results from 225 Live Days of XENON100 Data," Phys. Rev. Lett. **109**, 181301 (2012) [arXiv:1207.5988 [astro-ph.CO]].

[7] D. S. Akerib *et al.* [LUX Collaboration], "First results from the LUX dark matter experiment at the Sanford Underground Research Facility," arXiv:1310.8214 [astro-ph.CO].

[8] R. Agnese *et al.* [SuperCDMS Collaboration], "Search for Low-Mass WIMPs with SuperCDMS," arXiv:1402.7137 [hep-ex].

[9] E. Aprile [XENON1T Collaboration], "The XENON1T Dark Matter Search Experiment," arXiv:1206.6288 [astro-ph.IM].

[10] M. Felizardo, T. A. Girard, T. Morlat, A. C. Fernandes, A. R. Ramos, J. G. Marques, A. Kling and J. Puibasset *et al.*, "Final Analysis and Results of the Phase II SIMPLE Dark Matter Search," Phys. Rev. Lett. **108**, 201302 (2012) [arXiv:1106.3014 [astro-ph.CO]].

[11] S. Archambault *et al.* [PICASSO Collaboration], "Constraints on Low-Mass WIMP Interactions on ^{19}F from PICASSO," Phys. Lett. B **711**, 153 (2012) [arXiv:1202.1240 [hep-ex]].

[12] E. Behnke *et al.* [COUPP Collaboration], "First Dark Matter Search Results from a 4-kg CF_3I Bubble Chamber Operated in a Deep Underground Site," Phys. Rev. D **86**, 052001 (2012) [arXiv:1204.3094 [astro-ph.CO]].

[13] T. Tanaka *et al.* [Super-Kamiokande Collaboration], "An Indirect Search for WIMPs in the Sun using 3109.6 days of upward-going muons in Super-Kamiokande," Astrophys. J. **742**, 78 (2011) [arXiv:1108.3384 [astro-ph.HE]].

[14] R. Abbasi *et al.* [IceCube Collaboration], "Multi-year search for dark matter annihilations in the Sun with the AMANDA-II and IceCube detectors," Phys. Rev. D **85**, 042002 (2012) [arXiv:1112.1840 [astro-ph.HE]].

[15] P. J. Fox, R. Harnik, J. Kopp and Y. Tsai, "Missing Energy Signatures of Dark Matter at the LHC," Phys. Rev. D **85**, 056011 (2012) [arXiv:1109.4398 [hep-ph]].

[16] M. Doro *et al.* [CTA Collaboration], "Dark Matter and Fundamental Physics with the Cherenkov Telescope Array," Astropart. Phys. **43**, 189 (2013) [arXiv:1208.5356 [astro-ph.IM]].

[17] H. An, X. Ji and L. T. Wang, "Light Dark Matter and Z' Dark Force at Colliders," JHEP **1207**, 182 (2012) [arXiv:1202.2894 [hep-ph]].